



Spectroscopy of indoles in argon matrices at 20K, with 1La origin identification
by Bruce Jonathon Fender

A thesis submitted in partial fulfillment of the requirements for the degree of Doctor of Philosophy in
Chemistry

Montana State University

© Copyright by Bruce Jonathon Fender (1997)

Abstract:

The first site selected UV spectra (with polarization) of matrix isolated indole, 3-methylindole, 5-methylindole, 2-methylindole, 1-methylindole, 2,3-dimethyl indole, and 4-fluoroindole in argon at 20K were obtained. The main thrusts of this research is to locate the true 1La origin, and to characterize the fluorescence and the phosphorescence.

The true 1La origin for indole lies $1100-1300\text{ cm}^{-1}$ (split) above the 1Lb origin and the true 1La origin was distinguished from its false 1La origin at 455 and 480 cm^{-1} (jet). The fluorescence was identified as 1Lb and sharp (10 cm^{-1}) phosphorescence was obtained giving the Franck-Condon factors for La emission. The 1La origin for 3-methylindole was 260 cm^{-1} (unsplit) above the 1Lb origin, which was verified both by fluorescence anisotropy and 2-photon measurements. The fluorescence was identified as 1Lb. For 2,3-dimethylindole the combined perturbation of the two methyl groups causes the inversion of states with the 1La being 190 cm^{-1} below the 1Lb. This was verified by 1La fluorescence identification and by 2-photon measurements. The 1La fluorescence can be distinguished from its 1Lb counterpart.

The rest of the mono-methylated indoles emit from the 1Lb state and the 1La origin lies above the 1Lb as follows: 5-methylindole (1800 cm^{-1}), 2-methylindole ($400-600\text{ cm}^{-1}$), 1-methylindole ($430-600\text{ cm}^{-1}$). For 4-fluoroindole the 1La origin lies 1520 cm^{-1} above the 1Lb and the fluorescence is characterized by a long Franck-Condon progression of the $26^{\circ}1$ mode.

Also included in this work is indole and 3-methylindole in N_2 at 30K, 3-methylindole in ethanol at 15K, and 3-methylindole complexed with H_2O and methanol in a supersonic jet.

This information will facilitate the use of tryptophan as a spectroscopic probe molecule in the understanding of protein structure and dynamics.

**SPECTROSCOPY OF INDOLES IN ARGON MATRICES AT 20K,
WITH 1La ORIGIN IDENTIFICATION**

by

Bruce Jonathon Fender

**A thesis submitted in partial fulfillment
of the requirements for the degree**

of

Doctor of Philosophy

in

Chemistry

**MONTANA STATE UNIVERSITY
Bozeman, Montana**

July, 1997

D378
F3522

APPROVAL

of this thesis submitted by

Bruce Jonathon Fender

This thesis has been read by each member of the thesis committee and has been found to be satisfactory regarding content, English usage, format, citations, bibliographic style, and consistency, and is ready for submission to the College of Graduate Studies.

July 23, 1997
Date

Patrick R. Callis
Chairperson, Graduate Committee

Approved by the Major Department

July 24, 1997
Date

David M. Wiley
Head, Major Department

Approved for the College of Graduate Studies

7/27/97
Date

R. Bro
Graduate Dean

STATEMENT OF PERMISSION TO USE

In presenting this thesis in partial fulfillment of the requirement for a doctoral degree at Montana State University, I agree that the library shall make it available to borrowers under rules of the library. I further agree that copying of this thesis is allowable only for scholarly purposes, consistent with "fair use" as prescribed in the U. S. Copyright Law. Requests for extensive copying or reproduction of this thesis should be referred to University Microfilm International, 300 North Zeeb Road, Ann Arbor, Michigan 48106, to whom I have granted "the exclusive right to reproduce and distribute my dissertation in and from microform along with the non-exclusive right to reproduce and distribute my abstract in any format in whole or in part."

Signature *Bonnie J. French*

Date 7/23/97

ACKNOWLEDGMENTS

I wish to thank Professor Patrik Callis for his guidance, support, and insight, which has kept me on track during my graduate career. I thank the Callis group, especially Dr. Pedro Muino, Kurt Short, and David Hahn, for their advice and assistance during my stay in the group.

I also wish to thank Professor Lee Spangler and his group for their willingness to give a helpful word of advice or the lending of equipment.

I would also like to thank the rest of the members of my graduate committee, Dr. Reed Howald, Dr. Jan Sunner, Dr. Eric Grimsrud, and Dr. Myles Watts for their time and commitment.

And a final word of thanks goes to my family (to my Mom and Dad, to my brother and his family, and to my sister) for their constant love and support through the years.

TABLE OF CONTENTS

	Page
LIST OF TABLES	vii
LIST OF FIGURES	viii
ABSTRACT	xii
1. INTRODUCTION	1
Background	4
Statement of Problem	11
2. THEORY	14
Emission Anisotropy	14
The Onsager-Mataga-Lippert Model	16
Herzberg-Teller Coupling	18
Fermi Resonance	20
Site Selective Spectroscopy	21
Phosphorescence	25
Principles of Supersonic Jet Spectroscopy	28
Two-Photon Spectroscopy	29
3. EXPERIMENTAL SECTION	34
Matrix Isolation	34
Absorption Measurements	39
Phosphorescence Measurements	41
Two-Photon Spectroscopy	41
Formation of the Matrices	42
Supersonic Jet Instrument	45
4. RESULTS AND DISCUSSION	49
Indole in an Argon Matrix	49
Fermi Resonance	56

TABLE OF CONTENTS-Continued

	Page
Herzberg-Teller	59
The 1L_a Origin	60
Site Structure	63
Phosphorescence	68
3-Methylindole	74
5-methylindole	84
2,3-Dimethylindole	86
2-Methylindole	96
1-Methylindole	98
Phosphorescence	104
4-Fluoroindole	106
Phosphorescence	118
Comparison Of Properties	120
Nitrogen	124
Indole in N_2 at 30K	124
3-Methylindole in N_2 at 30K	129
3-Methylindole in Ethanol at 15K	131
3-Methylindole Complexes in a Supersonic Jet	135
Water Complex	135
Methanol Complex	139
5. SUMMARY	146
REFERENCES	148

LIST OF TABLES

Table	Page
1. The two-photon values of the argon matrix and the jet spectra	54
2. Indole Phosphorescence	73
3. 1-Methylindole phosphorescence	105
4. 4-Fluoroindole phosphorescence	119
5. The energy difference for the 1L_a and 1L_b states of substituted indoles relative to indole	121
6. The frequencies of modes 28, 27, 26	121
7. Site energies for the S_1 , S_2 , T_1 states of indole in argon at 20K	122
8. Indole + H_2O	139
9. Indole + Methanol	142

LIST OF FIGURES

Figures	Page
1. Tryptophan	3
2. Indole with numbering system	3
3. Excitation to the 1L_a and 1L_b states, where r is a distortion along a general coordinate that takes the geometry from the 1L_b minimum to the 1L_a minimum	5
4. Schematic diagram for determining the emission anisotropy	15
5. Site structure of the supersonic jet environment, (a), argon matrix environment, (b), and solution environment, (c)	23
6. Phosphorescence (Ph) and fluorescence (Fl)	27
7. Supersonic jet expansion	28
8. One and two-photon spectroscopy	30
9. Matrix isolation experimental setup	35
10. Transmittance experimental setup	40
11. Jet experimental setup	48
12. Transmittance spectrum of indole in argon at 20K, with 0.2 cm^{-1} bandpass	50
13. The 26^0_1 line excited at 285.84, 285.85, 285.86, 285.87, 285.88 nm, with a 2 cm^{-1} bandpass	51
14. Supersonic jet fluorescence excitation spectrum of indole (with Ω values), (a), simulated matrix spectrum, (b), fluorescence excitation spectrum of indole in argon at 20K, (c), and the fluorescence anisotropy, (d)	53

LIST OF FIGURES-Continued

	Page
15. Two-photon spectrum of the 1L_b origin, (a), 26^1_0 , (b), and 28^1_0 , (c), of indole in argon at 20K	55
16. Fermi resonance of the 29^1_0 and the $41^1_0, 42^1_0$ lines	59
17. Fluorescence spectrum of indole in argon at 20K ($500-800\text{ cm}^{-1}$), (a), and fluorescence anisotropy, (b)	61
18. Fluorescence spectrum of indole in argon at 20K, (a), and the stick spectrum, (b)	64
19. Fluorescence excitation spectra ($200-1400\text{ cm}^{-1}$) of indole in argon at 20K from site 1, (a), site 2, (b), site 5, (c), and site 3, (d)	67
20. The phosphorescence decay, (a), and the log plot, (b)	68
21. The phosphorescence spectra of indole in argon at 20K from site 1, (a), site 5, (b), and site 2, (c)	71
22. The phosphorescence spectrum of indole in argon at 20K from site 5, (a) and the stick spectrum	72
23. Transmittance spectrum of 3MI in argon at 20K, with a 0.2 cm^{-1} bandpass	75
24. Supersonic jet fluorescence excitation spectrum of 3MI (with Ω value), (a), fluorescence excitation spectrum of 3MI in argon at 20K, (b), and fluorescence anisotropy, (c)	78
25. Two-photon spectrum of the 1L_a and 1L_b origin region ($-50-400\text{ cm}^{-1}$) of 3MI in argon at 20K	79
26. Dispersed fluorescence spectrum of 3MI in argon at 20K	82
27. Dispersed phosphorescence spectrum of 3MI in argon at 20K, with 1L_b origin excitation at 288.78 nm	83

LIST OF FIGURES-Continued

	Page
28. Supersonic jet fluorescence excitation spectrum of 5MI (with Ω values), (a), fluorescence excitation spectrum of 5MI in argon at 20K, (b), and fluorescence anisotropy, (c)	87
29. Dispersed fluorescence spectrum of 5MI in argon at 20K	88
30. Dispersed phosphorescence spectrum of 5MI in argon at 20K, with 1L_b origin excitation at 291.75 nm	89
31. Fluorescence excitation spectrum of 2,3DMI in argon at 20K, (a), and the fluorescence anisotropy, (b)	93
32. Dispersed fluorescence spectrum of 2,3DMI in argon at 20K	94
33. Dispersed phosphorescence spectrum of 2,3DMI in argon at 20K, with 1L_a origin excitation at 288.66 nm	95
34. Transmittance spectrum of 2MI in argon at 20K, with a 0.2 cm^{-1} bandpass	99
35. Fluorescence excitation spectrum of 2MI in argon at 20K, (a), and the fluorescence anisotropy, (b)	100
36. Dispersed fluorescence spectrum of 2MI in argon at 20K	101
37. Dispersed phosphorescence spectrum of 2MI in argon at 20K, with 1L_b origin excitation at 286.07 nm	102
38. Transmittance spectrum of 1MI in argon at 20K, with a 0.2 cm^{-1} bandpass	107
39. Fluorescence excitation spectrum of 1MI in argon at 20K, (a), and the fluorescence anisotropy, (b)	108
40. Dispersed fluorescence spectrum of 1MI in argon at 20K	109
41. Dispersed phosphorescence spectrum of 1MI in argon at 20K, with 1L_b origin excitation at 291.55 nm, and stick spectrum, (b)	110

LIST OF FIGURES-Continued

	Page
42. Transmittance spectrum of 4FI in argon at 20K, with a 0.2 cm ⁻¹ bandpass	114
43. Fluorescence excitation spectrum of 4FI in argon at 20K, (a), and fluorescence anisotropy, (b)	115
44. Dispersed fluorescence spectrum of 4FI in argon at 20K	116
45. Dispersed phosphorescence spectrum of 4FI in argon at 20K, with ¹ L _b origin excitation at 281.89 nm, (a), and the stick spectrum, (b) ..	117
46. Energies of the ¹ L _a and ¹ L _b states	123
47. The fluorescence excitation spectrum of indole in N ₂ at 30K, (a), and the fluorescence anisotropy, (b)	126
48. Fluorescence spectra of indole in N ₂ at 30K, (a), and N ₂ at 15K, (b) ...	127
49. The phosphorescence spectrum of indole in N ₂ at 30K	128
50. Transmittance spectra of 3MI in argon at 20K, (a) and N ₂ at 30K, (b) ..	130
51. Fluorescence spectra of 3MI in ethanol at 300K, (a), 15K, (b), and red-edge excitation (307 and 303.5 nm) at 15K, (c)	134
52. The fluorescence excitation spectrum of 3MI(H ₂ O) ₁ in a supersonic jet (with Ω values)	137
53. Two-photon spectrum of 3MI(H ₂ O) ₁ complex origin (with Ω values)	138
54. The fluorescence excitation spectrum of 3MI(methanol) ₁ in a supersonic jet (with Ω values)	143
55. Two-photon spectra of the bare 3MI origin, (a), and 3MI(methanol) ₁ complex origin, (b), (with Ω values)	144
56. Two-photon spectra of the first quanta at -268.3 cm ⁻¹ , (a), and the second quanta at -247.2 cm ⁻¹ , (b), (with Ω values)	145

ABSTRACT

The first site selected UV spectra (with polarization) of matrix isolated indole, 3-methylindole, 5-methylindole, 2-methylindole, 1-methylindole, 2,3-dimethylindole, and 4-fluoroindole in argon at 20K were obtained. The main thrusts of this research is to locate the true 1L_a origin, and to characterize the fluorescence and the phosphorescence.

The true 1L_a origin for indole lies 1100-1300 cm^{-1} (split) above the 1L_b origin and the true 1L_a origin was distinguished from its false 1L_a origin at 455 and 480 cm^{-1} (jet). The fluorescence was identified as 1L_b and sharp (10 cm^{-1}) phosphorescence was obtained giving the Franck-Condon factors for L_a emission. The 1L_a origin for 3-methylindole was 260 cm^{-1} (unsplit) above the 1L_b origin, which was verified both by fluorescence anisotropy and 2-photon measurements. The fluorescence was identified as 1L_b . For 2,3-dimethylindole the combined perturbation of the two methyl groups causes the inversion of states with the 1L_a being 190 cm^{-1} below the 1L_b . This was verified by 1L_a fluorescence identification and by 2-photon measurements. The 1L_a fluorescence can be distinguished from its 1L_b counterpart.

The rest of the mono-methylated indoles emit from the 1L_b state and the 1L_a origin lies above the 1L_b as follows: 5-methylindole (1800 cm^{-1}), 2-methylindole (400-600 cm^{-1}), 1-methylindole (430-600 cm^{-1}). For 4-fluoroindole the 1L_a origin lies 1520 cm^{-1} above the 1L_b and the fluorescence is characterized by a long Franck-Condon progression of the 26^0_1 mode.

Also included in this work is indole and 3-methylindole in N_2 at 30K, 3-methylindole in ethanol at 15K, and 3-methylindole complexed with H_2O and methanol in a supersonic jet.

This information will facilitate the use of tryptophan as a spectroscopic probe molecule in the understanding of protein structure and dynamics.

Chapter 1

INTRODUCTION

Proteins are one of the basic building blocks of life consisting of chains of amino acids linked together through amide bonds. One amino acid is distinguished from another by its side chain. Protein chemistry is quite complex; the sequence and conformation of amino acids of proteins are needed to completely understand its functionality. There are many ways of understanding protein conformation: from a theoretical standpoint using molecular modeling and dynamic simulations or from an experimental standpoint using NMR, X-ray crystallography, and spectroscopy. A common technique, X-ray diffraction, obtains a three-dimensional structure but requires the protein to be crystalline, which is quite difficult to nearly impossible for certain proteins. Furthermore, since the protein is not in its natural environment, the information gained is questionable when extended to living systems. This technique is also unable to study conformational changes in proteins due to environmental changes.

Spectroscopic techniques, where light is used to interact with an environmentally sensitive probe molecule, revealing structural and environmental information about the protein in vivo (living systems), offers useful complementary information. Three amino acids could be used as natural

spectroscopic probes in proteins when monitoring fluorescence with UV excited light: tyrosine, tryptophan, and phenylalanine. However, tyrosine is insensitive to its local environment and phenylalanine has a poor quantum yield.

Furthermore, if tryptophan was present in the residue, then observing the fluorescence from either tyrosine or phenylalanine would be difficult.

Tryptophan, on the other hand, is a more sensitive probe because of its low-lying 1L_a excited state, whose large permanent dipole interacts strongly with its local environment^{1,2}. Tryptophan can also be selectively excited on the long-wavelength absorption edge. For these reasons tryptophan has served as a spectroscopic probe molecule in proteins for over 30 years¹. The structure of tryptophan in its zwitterion state is shown in Figure 1.

Tryptophan is naturally incorporated in many proteins, and it may be inserted by point mutations if needed. Indole, the chromophore of the amino acid tryptophan, accounts for much of the UV absorption of proteins. The structure of indole and its numbering system is shown in Figure 2. Indole has two low lying $\pi\pi^*$ singlet excited states, labeled 1L_a and 1L_b , using Platt notation³. The overlap of these nearly degenerate states causes the absorption spectrum to be quite complicated. A considerable amount of experimental and theoretical data on indole exists^{1,2,4-19,21-23}, but because of its complicated nature, its spectroscopic properties are still not fully known. Consequently, a more comprehensive picture of the electronic structure of indole is needed.

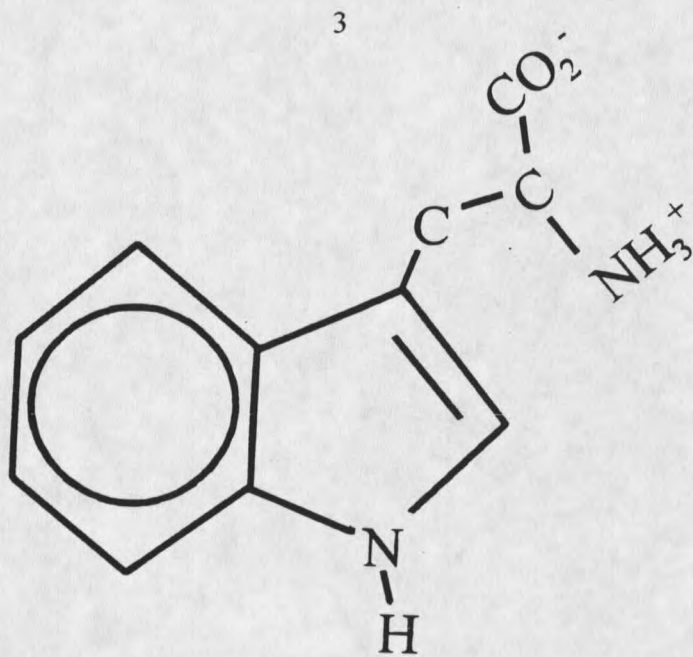


Figure 1. Tryptophan

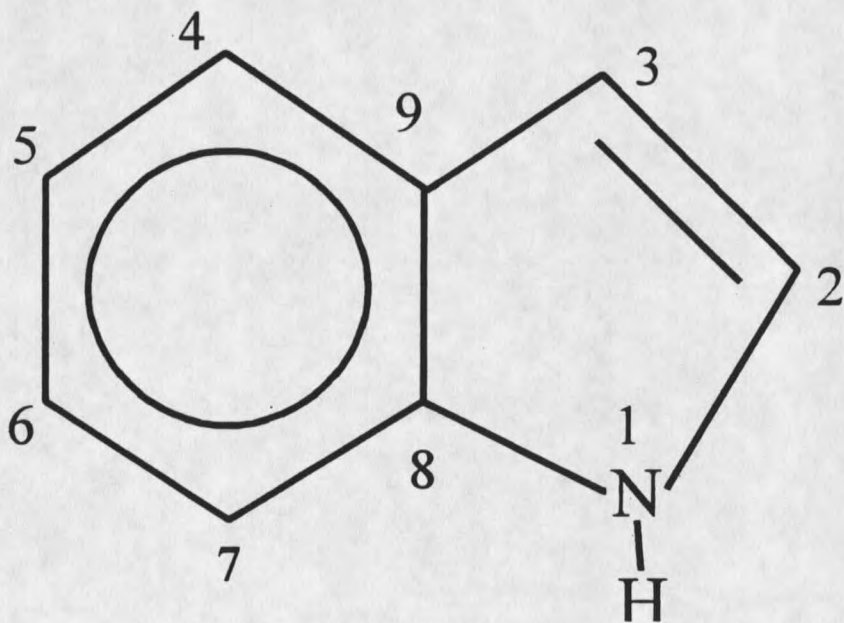


Figure 2. Indole with numbering system.

Background

In 1976, Valeur and Weber completed work on indole in propylene glycol at -58°C with polarized emission⁴. They concluded from the emission anisotropy that the 280 nm band consisted of two excited states, 1L_a and 1L_b , whose transition moments lie in the plane of the molecule at approximately 90° relative to each other (see Figure 3). They went on to separate and resolve the two excited states using the anisotropy. However, their experiment lacked resolution, so they could not resolve individual vibrational lines.

The 1L_b state of indole is known to have a smaller geometry change upon excitation and a permanent dipole similar to the ground state⁵. Therefore, the 1L_b state is less perturbed by its local environment and can be recognized by its relatively sharp structure. The 1L_b state is the S_1 state for indole, 5-methylindole (5MI), and 3-methylindole (3MI) in a nonpolar (low-interacting) environment.

The 1L_a state, on the other hand, has a large permanent dipole because its transition involves charge transfer, where electron density is shifted from the 5-member ring to the 6-member ring^{5,72}. This increase in dipole causes its fluorescence to be red-shifted and broadened by large Stokes shifts because of the larger interaction between its permanent dipole and the environment. These two factors cause the 1L_a state in solution to be recognized by its broad structure. In a polar environment, the 1L_a state will be the S_1 state for indole, 3MI, and 2,3-dimethylindole (2,3DMI). 5MI is one exception and emits from

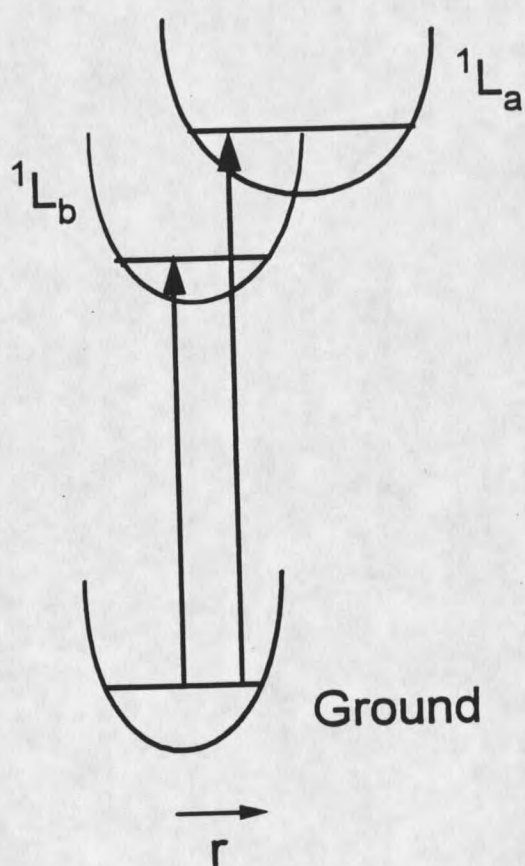


Figure 3. Excitation to the 1L_a and 1L_b states, where r is a distortion along a general coordinate that takes the geometry from the 1L_b minimum to the 1L_a minimum.

both states in a polar environment ⁶.

Comparing vapor phase spectra and partially resolved room temperature solution spectra, Strickland *et al.*^{7,8} have given evidence for these two electronic states in indole and indole derivatives (3MI and 2,3DMI). The ¹L_a lines were distinguished from the ¹L_b lines by differential solvent shifts due to their differences in permanent dipole and differences in dispersion interactions. The ¹L_a origin of indole was postulated to lie 1460 cm⁻¹ above the ¹L_b origin in the vapor. They first noted that methylation in the 3-position caused significant changes to the absorption spectrum; the ¹L_a origin was found to be extremely sensitive to this methylation, drastically red-shifting to 680 cm⁻¹ above the ¹L_b origin in vapor and 340 cm⁻¹ in perfluorohexane. The Callis group verified the latter result with a value of 300 cm⁻¹ in perfluorohexane, using a 2-photon technique⁹. By the addition of a second methyl group to indole in the 2-position producing 2,3DMI, further red-shifts the ¹L_a origin. Strickland *et al.*⁷ concluded that the ¹L_a and the ¹L_b origins nearly overlap both in vapor and in perfluoromethylcyclohexane. This evidence points toward substitutions and solvation playing an important role in the photophysics of indole.

Utilizing supersonic jet spectroscopy, Wallace and coworkers have done extensive spectroscopy on indole and indole derivatives as isolated molecules or molecular complexes¹⁰⁻¹⁶. They used a variety of experimental techniques in their thorough investigation of indole: nanosecond fluorescence excitation, picosecond 2-photon resonant ionization, lifetime measurements via picosecond

excitation, and dispersed emission. Extensive lifetime measurements of the excited state were made and attempts were made to use lifetimes as a method to distinguish 1L_b states with longer lifetimes from 1L_a states with shorter lifetimes. This method reveals lifetimes, but lifetime measurements cannot be used as a positive means of identifying the state. There tends to be a general connection between the 1L_a - 1L_b energy gap and the lifetimes, where smaller 1L_a - 1L_b energy gaps produce shorter lifetimes and vice versa. These experiments simply tuned the 1L_a - 1L_b energy gap of indole by methylation and/or complexation. Through this work, Wallace *et al.*^{13,16}, and Lami and Glasser^{84,65} suggested that the 1L_a state is a nonradiative state through dissociation of the N-H bond. However, this nonradiative mechanism was later experimentally proven incorrect¹⁷.

Callis and coworkers made huge strides in the development of a 2-photon technique, which had the ability to separate 1L_a lines from 1L_b lines through the absorption event. The two photon technique used the preferential absorption of circular versus linear polarized light, where the polarization ratio Ω can be measured, where Ω =intensity using circular polarized light/intensity using linear polarized light. For an 1L_b transition the $\Omega \sim 1.5$ and for an 1L_a transition the $\Omega \sim 0.5$ ^{9,18,21}. The absorption of the two photons happens on the femtosecond time scale; therefore, this technique can be used under nonrigid conditions such as liquids and gases because the two photons absorb before the molecule loses its orientation due to rotational motion. This method has had profound ability to separate 1L_a and 1L_b states in the excited state manifold, except vibronically

coupled lines. The method was first applied to indole and indole derivatives in various solvents at room temperature¹⁸ and subsequently used on indole vapor^{19,20} and 3MI vapor²⁰, where the 1L_a intensity was found 1454cm^{-1} above the 1L_b origin for indole and 400cm^{-1} for 3MI.

The recent expansion of supersonic jet spectroscopy, and in conjunction with this two-photon technique gave the experimenter the highest resolution and the clearest picture of the two excited states. The Callis group completed many experiments on a variety of indoles (indole, 3MI, (d_1 -3MI), and 5MI); the positions of the 1L_a and 1L_b lines were located and identified, and a picture was made between methylation and the 1L_a and 1L_b states. For the first time, a more definitive statement could be made concerning these two states.

Indole had two small lines at 455 and 480cm^{-1} above the 1L_b origin that gave an 1L_a signature, but most of the 1L_a intensity sat 1000cm^{-1} higher in energy. It was first speculated that these two lines were in fact the 1L_a origin and were split (25cm^{-1} splitting) by coupling to the nearby 1L_b origin, but there was much hesitation about this assignment. First, the combined intensity of these two lines was much lower than the intensity of the 1L_b origin. This result was later contradicted by theory⁵. Second, it was theorized that these lines were not the 1L_a origin, but vibronically coupled 1L_b lines. Bickel *et al.*¹⁰ performed extensive dispersed fluorescence experiments on indole in a jet, using ground state assignments, then assigning the corresponding excited state frequencies; the 480cm^{-1} line was assigned 28^1_0 and the 455cm^{-1} line was assigned $39^1_{0,41}1_0$.

These lines were not assigned to a different origin. Later experiments involving hydrogen bonded complexes in the jet were completed to shed light on this assignment²¹. It was postulated that the 1L_a lines should have a greater red-shift upon complexation than corresponding 1L_b lines due to their difference in permanent dipole. Upon complexation (methanol, H_2O , and D_2O), the 480 cm^{-1} and 455 cm^{-1} lines of indole did not red-shift relative to the complexes' origin, but the intensities of the lines varied. The lines not red-shifting gave evidence for vibronic coupling, and the line intensity variation gave evidence for Fermi resonance.

The 1L_a origin of 3MI lies in several lines between $300\text{-}900\text{ cm}^{-1}$ above the 1L_b origin, with no discernable prominent 1L_a origin. The 1L_a origin is split due to coupling to the 1L_b manifold. Also, the methyl rotor is inactive on excitation. For 5MI, the 1L_a intensity lies approximately 1400 cm^{-1} above the 1L_b origin, and the methyl rotor is active upon excitation with a 60° conformational change of the methyl group²². This coupling lowers the line intensity because the intensity is distributed over the entire methyl rotor structure.

Due to the popularity of using tryptophan as a spectroscopic probe, currently several tryptophan analogues are being used as optical probes in proteins in replacement of tryptophan²³⁻²⁶. One of these analogues is 4-fluorotryptophan (4-FT), where 4-fluoroindole (4FI) replaces indole as the chromophore²³. The purpose of this change is to select the desired emission characteristics by selecting the desired chromophore. 4-FT was selected

because it could be naturally incorporated into proteins in the place of tryptophan did not change the functionality of the protein, and would not fluoresce. In practice, one or more of the tryptophan(s) in a protein containing multiple tryptophans could in essence be "turned off" with the goal of unraveling a complex fluorescence spectrum by selectively deleting emitters. Because of this characteristic, there is a renewed interest in understanding fluorinated indoles^{27,28}.

Low temperature glasses/matrices have been studied for the last several decades. Low temperature matrices have given experimenters the ability to study reactive species, radicals, and ions²⁹⁻³¹, which would be nearly impossible to study otherwise. In recent years, there has been a renewed interest in matrix isolated spectroscopy with the advent of narrow band laser excitation sources, which selectively excite molecules that are in a narrow range of energy, giving site selection capabilities. The matrix material ranges from noble gases (as in this thesis) to various hydrocarbons made popular by Shpol'skii^{32,33}.

Indole has also been studied in low temperature glasses. As mentioned earlier, Valeur and Weber studied indole and various related compounds in propylene glycol at -58°C. Kawski *et al.*³⁴ did room temperature study on indole incorporated in a poly(vinyl alcohol) film, with polarized fluorescence and phosphorescence. Illich *et al.* studied indole in an argon matrix at 10K, but was unable to select from a single site³⁵. This experiment gave a blurred excitation spectrum that consisted of several spectra on top of one another.

The research that influenced our decision to explore indole in argon was completed by Gutmann *et al.*³⁶, who studied naphthalene and octadeutonaphthalene in argon at 12K, with both one and two-photon techniques. They could produce extremely sharp lines, some as narrow as 4 cm^{-1} , which could compete with the resolution of the jet. Gupiapati *et al.*³⁷ later studied anthracene and pyrene in argon with polarized emission measurements. These experiments gave us the evidence we needed: argon matrices can produce sharp lines and polarized emission.

Statement Of The Problem

Previous research has positively identified 1L_a transitions in various indoles; the two-photon technique incorporated with jet expansion has given a high resolution picture of the excited state manifold of various indoles. Still, there has been no positive identification of the 1L_a origin for indole, 3MI, d_3 -3MI, and 5MI, using 2-photon spectroscopy because it cannot distinguished between true 1L_a lines and vibronically coupled 1L_b lines.

In indole, there is speculation that the 480 cm^{-1} and 455 cm^{-1} lines do not constitute the true 1L_a origin, but a split false origin. For 3MI, there is no discernable prominent 1L_a origin; instead the intensity is spread over several lines spanning 400 cm^{-1} . For 5MI, the 1L_a origin is well above the 1L_b origin, but the exact location has not been found. For 2,3DMI the 1L_a origin is supposed to be near the 1L_b origin, and for 2MI, 1MI, and 4FI the 1L_a origins are completely

unknown.

In proteins there is some uncertainty with fluorescence, because of two possible fluorescent states of indole. For indole, polar environment favors 1L_a emission, and nonpolar favors 1L_b emission; however, proteins lie somewhere between these extremes. A question remains about the existence of sharp 1L_a fluorescence and its structure. Fluorescence monitoring is an experimental aid in the understanding of protein chemistry, and there is a common practice: if the fluorescence is sharp then it is considered to be 1L_b , but if the fluorescence is diffuse then it is considered to be 1L_a fluorescence. This assumption may be flawed. There is no fundamental reason there could not be sharp 1L_a fluorescence, except that the conditions that are conducive to producing 1L_a fluorescence, i.e. polar environments, are also conducive to broadening it. If an incorrect fluorescence assignment of a protein is made, then false information about the protein environment is given. Theoretical results have shown some significant differences between 1L_a and 1L_b emission due to differences in Franck-Condon factors between the two excited state potentials and the ground state potential³⁸, but experimental verification is needed.

This research will use site selective matrix isolation of indole, 3MI, 5MI, 2,3DMI, 2MI, 1MI, and 4FI to unravel the complex photophysics of indole. Site selection produces sharp lines, and matrix isolation produces a rigid trapping environment, where photoselection leads to anisotropic emission. This method incorporates a small-bandpass laser in conjunction with a small-bandpass

monochromator, giving the experimenter the ability to produce sharp fluorescence excitation, fluorescence, and phosphorescence spectra. This technique can distinguish between 1L_a and 1L_b states by emission anisotropy and by differential solvent shift. The differential shift will be able to separate false 1L_a lines (vibronically coupled lines) from true 1L_a lines. This technique can help complete the picture painted by the jet and positively identify the true 1L_a origins, identify the emission, and examine the phosphorescence. This data will also give pertinent information as to how substitutions to the indole ring affect both the electronic energies of the 1L_a and 1L_b states and normal modes frequencies.

Chapter 2

THEORY

Emission Anisotropy

The emission anisotropy measurements are critical to the experiments carried out in this thesis. The discussion will follow the theory laid out by Kawski³⁹ and will depend on these four basic assumptions:

- 1) Considering the case of linear polarized excitation of a dilute fluorophore in a rigid environment, where rotation between excitation and emission is impossible.
- 2) There is no phase relation between the exciting light and the emitting light.
- 3) The direction of the emission transition dipole, relative to the molecular axis, does not depend on the excitation, but only on the molecular states between which the transition occurs.
- 4) No other depolarizing factors will be taken into account.

Consider the case of an excitation vector, E , vertically polarized along the x-axis, see Figure 4.

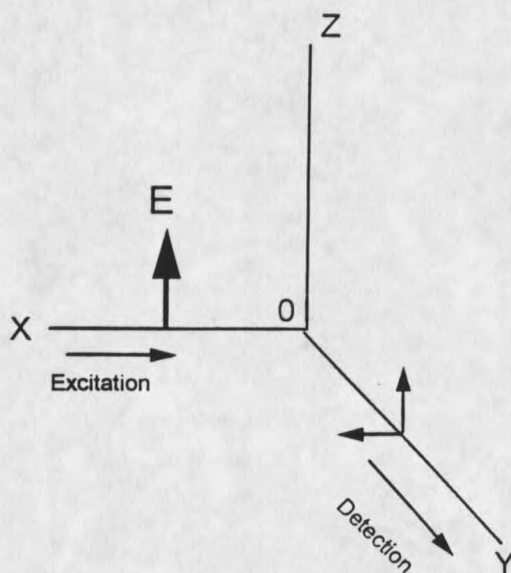


Figure 4. Schematic diagram for determining the emission anisotropy.

According to Jablonski⁴¹, the anisotropy of the emission, r , for the emission field can be defined as:

$$r = \frac{I_{\parallel} - I_{\perp}}{I_{\parallel} + 2I_{\perp}} \quad (1)$$

Equation 1 is used in the laboratory to calculate the anisotropy of the emission.

The denominator is proportional to the total emission intensity. The

perpendicular term can be factored out using the following relation $I_{\perp} = (I - I_{\parallel})/2$

giving Equation 2:

$$r = \frac{3}{2} \cdot \frac{I_{\parallel}}{I} - \frac{1}{2} \quad (2)$$

Equation 2 is expanded to incorporate the angular dependence of the absorption and emission moments on the anisotropy giving the Perrin equation⁴⁰:

$$r(\beta) = \frac{2}{5} \left[\frac{3}{2} \cos^2 \beta - \frac{1}{2} \right], \quad (3)$$

where β is the angle between the absorption and emission moments. For a complete discussion see Kawski³⁹. The first part of Equation 3 is the maximum anisotropy due to photoselection, $2/5$, and the second part in brackets is the angular dependence of anisotropy. The emission anisotropy (r) will have values ranging from -0.2 to 0.4 , for $\beta = 90^\circ$ and $\beta = 0^\circ$, respectively. These are the theoretical values and the experimental values will deviate somewhat due to depolarization in the experiment. If depolarization does occur, then it is important check for the anisotropy values be at the proper ratio ($2:-1$).

The Onsager-Mataga-Lippert Model

The Onsager-Mataga-Lippert Model⁴²⁻⁴⁹ will be used as a method of calculating spectral shifts that result from the solute molecule placed in a medium with a constant dielectric constant (ϵ). This model is based on the Onsager reaction field. The model is used to calculate the energy correction for absorption in vacuum compared with absorption in a solvent. The model is based on the representation of the solute molecules as point dipoles, with both the ground state dipole, μ_g , and the excited state dipole, μ_e , in a solvent sphere

with a radius (a), a static dielectric constant (ϵ), and a refractive index (n), see Equation 4.

$$hc\Delta\bar{\nu}_{ground} = -(\mu_g)^2 \frac{2}{a^3} \left[\frac{\epsilon-1}{2\epsilon+1} - \frac{n^2-1}{2n^2+1} \right] - (\mu_g)^2 \frac{2}{a^3} \left[\frac{n^2-1}{2n^2+1} \right] \quad (4)$$

Equation 4 is broken into two terms, the first term corrects the energy due to the reaction field caused by the reorientation of the solvent. This does not change during excitation period of the solute, analogous to the Born-Oppenheimer approximation. This first term does not play a factor in the matrix experiments, because the matrix material does not have a permanent dipole and can be removed from the Equation 4. Even if there was a permanent dipole, the temperature and/or the rigidity of the matrix would not allow for this type of reorientational motion of the matrix.

The second term corrects the energy due to electronic polarizability of the solvent molecules. Since electrons are small, this electronic term is in equilibrium with the solvent molecules during the excitation period. The energy difference of excitation from the ground state to an excited state can be calculated as follows^{21,86}.

$$\Delta\bar{\nu}(cm^{-1}) = \frac{(\mu_e^2 - \mu_g^2)}{2} \frac{2}{a^3} \left[\frac{n^2-1}{2n^2+1} \right] * 5035, \quad (5)$$

where the numerical constant 5035 converts the energy change into cm^{-1} units⁸⁶. The first term is divide by two so that the free energy change is calculated and the equation requires the actual dipole⁸⁶. This model will be used to calculate the theoretical energy (free energy) shifts for the two excited states 1L_a and 1L_b , by the differences in their actual permanent dipoles.

This model is better suited for systems in polar solvents. For the argon matrix, this model is incomplete because it only deals with the more tangible permanent dipole difference and does not include a dispersion term. For molecules that do not have a permanent dipole by symmetry, these dispersion forces alone are responsible for the shifts. They can be quite large and are proportional to the polarizability of the solvent⁵⁰. The 1L_a state of naphthalene and anthracene is known to red-shift about 500 cm^{-1} more than the 1L_b state in hydrocarbon solvent⁵². Anthracene's 1L_a state is known experimentally to red-shift $500\text{-}700 \text{ cm}^{-1}$ by going into solid argon⁵¹ and red-shifts 1200 cm^{-1} further by incorporation into fluorene⁵³. It would be reasonable to expect part of the red-shift seen in the argon matrix to come from dispersion forces.

Herzberg-Teller Coupling

The intensity of a transition or the probability that a transition between two state occurs is proportional to the square of the transition dipole

$$I \propto |\bar{M}_{ge}|^2, \quad (6)$$

where I is the intensity of the transition and M_{ge} is the transition dipole between the ground state and the excited state. The transition dipole can be written explicitly:

$$\bar{M}_{ge} = \int \int \Psi_g(r, Q) \Phi_g(Q) \bar{M} \Psi_e(r, Q) \Phi_e(Q) dr dQ, \quad (7)$$

and can be rearranged

$$\bar{M}_{ge} = \int \Phi_g(Q) \left[\int \Psi_g(r, Q) \bar{M} \Psi_e(r, Q) dr \right] \Phi_e(Q) dQ, \quad (8)$$

where Ψ is the electronic wavefunction and Φ is the nuclear wavefunction, the subscripts g and e refer to the ground and excited states, respectively, and, r refers to the electronic coordinates and Q to the nuclear coordinates. The term in the square brackets is dependent on the nuclear coordinates and is constant under the Condon approximation. Herzberg-Teller vibronic coupling occurs when there is a failure of the Condon approximation and the term in the bracket needs to be expanded:

$$\bar{M}_{ge} = \int \Phi_g(Q) \left[\bar{M}_{ge}^0 + \sum_a \frac{\partial \bar{M}_{ge}}{\partial Q_a} Q_a + \dots \right] \Phi_e(Q) dQ, \quad (9)$$

where the first term is the transition dipole at the equilibrium position, and the second term has the vibronic coupling constants and is a function of nuclear

motion. Therefore, nuclear motion can couple intensity into a transition through this term.

Herzberg-Teller coupling occurs when a vibronic transition that is forbidden due to no displacement of the potential well, is observed due to nuclear displacement along a normal coordinate that comes from zero point vibrational motion of a ground state normal mode. If one of these modes has a non zero coupling constant, then the vibronic transition will be observed.

Fermi Resonance

Fermi resonance occurs when two vibrations are nearly degenerate in energy and in proper symmetry. This coupling occurs due to anharmonic behavior of the vibrations; one vibration interferes with the other, because they are not displaying 100% normal mode behavior. If they meet the proper symmetry conditions, then a perturbation can occur that mixes the two levels. This mixing causes intensity redistribution and splitting of these two levels, which depends on the energy separation and the interaction between the levels.

Fermi resonance can most easily be explained using the variation method rather than perturbation theory, because the interaction is typically beyond the perturbation limit. Fermi resonance can be explained by two cases of the variation method. In case 1 the energy levels are degenerate ($\alpha_1 - \alpha_2 = 0$) and in case 2 the energy separation is on the order of the interaction between the two states ($\alpha_1 - \alpha_2 \approx \beta$), where α_1 and α_2 are the energies of levels 1 and 2,

and β is the interaction between the levels. In case 1 there is an equal state mixing and in case 2 there is unequal state mixing. The wavefunction that describes the mixed states is a combination of the original wavefunctions. Through this mechanism, intensity can be redistributed from strongly allowed state and given to a weakly allowed state. Spectroscopists widely use Fermi resonance in data interpretation.

Site Selective Spectroscopy

Site selective spectroscopy is the technique used in these experiments to improve the spectral data. It is a method of acquiring spectral data from a matrix embedded sample that achieves the sharpest lines possible. This occurs because all the absorption and emission are from only one site, which sharpens and simplifies the spectra.

In a chemical system all molecules are perturbed by their local environment, the environment actually produces an electric field that the molecule senses. This field can interact with any changes made in the molecule, especially in the absorption and emission of photons. For a simple example, let us only consider a single electronic transition. The energy of such a transition will be designated by a vertical line in Figure 5. If the solvent field is oriented in such a way to facilitate the electronic transition, then the energy for the transition will red-shift to lower energy, but if the solvent field is opposed to the transition, the energy will blue-shift to higher energy. In solution there is a

"gaussian" distribution of environments; therefore, there is a "gaussian" distribution of perturbed molecules leading to broadening of the spectra, see Figure 5c. In the jet expansion there is a much smaller distribution of environments; the molecules are vibrationally and rotationally cold and isolated in a vacuum, see Figure 5a. This leads to narrow spectra. In the argon matrix at 20K there are several sites within the matrix, which are highly populated by the guest molecules, see Figure 5b. This can lead to narrow spectra. The term "site" selection is commonly used, but in actuality the correct term is "energy difference" selection or just "energy" selection.

First, site selection requires the guest molecule to be incorporated into a host matrix at a temperature well below the melting point of the host material. This low temperature of the matrix produces a rigid trapping environment for the guest molecule, where rotational structure and hot bands (hot bands are transitions caused by thermally excited molecules in the ground state.) are eliminated. The concentration of the guest molecule is kept low to reduce guest molecule/guest molecule interactions, so all environmental electronic influences come exclusively from the host matrix. Interaction (induced electric field) can be controlled, by controlling the polarizability of the matrix material. A less polarizable matrix should in theory interact less with the guest molecule and vice versa.

The basis behind site selection is that the guest molecule will occupy particular sites within the host matrix. Small guest molecules occupy interstitial

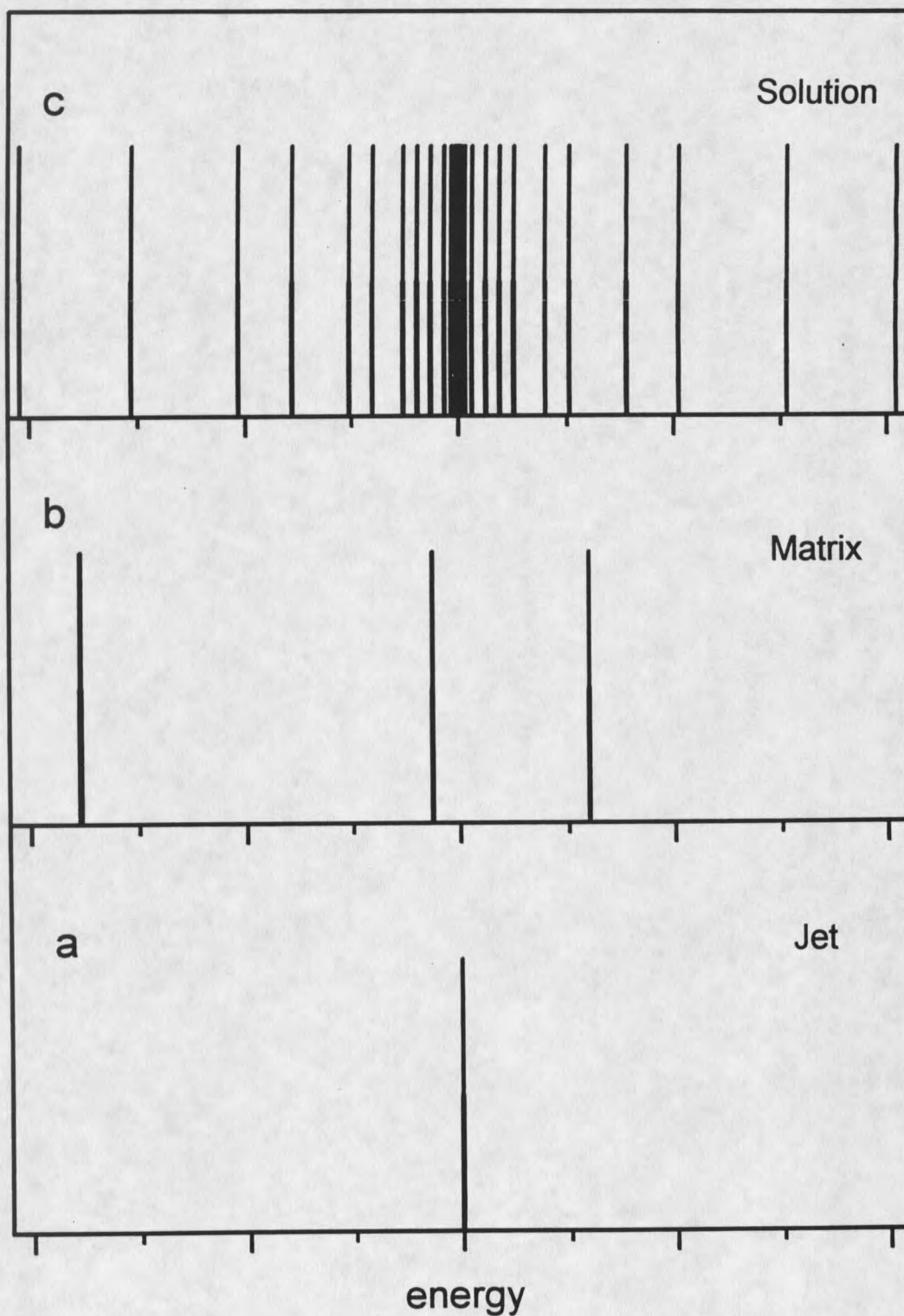


Figure 5. Site structure of the supersonic jet environment, (a), argon matrix environment, (b), and solution environment, (c).

holes (sites) that are analogous to those of the host molecules, and larger guest molecules occupy sites formed by actual displacement of one or more of the host atom(s) or molecule(s). In theory, these sites should be highly populated, with a large number of molecules sitting in a similar site (solvent cage) produced by a similar matrix arrangement around the guest molecules, producing similar molecular energies. There is extensive evidence of noble gas matrices having multiple sites in which aromatic molecules display transition energies differing about 100 cm^{-1} , which leads to band congestion in a conventional absorption spectroscopy. The reproducibility of the site structure in argon suggests that the argon matrix is indeed polycrystalline and indole fits into lattice planes within argon's the face center cubic (FCC) lattice structure by the removal of several argon atoms.

Second, to achieve site selection, the energy spacing between the sites must be far enough apart so that sites can be independently excited by a small bandpass laser, while monitoring a single vibrational line in the emission or vice versa. A small bandpass laser in conjunction with a small bandpass monochromator has the capabilities of producing sharp fluorescence excitation, dispersed fluorescence, and phosphorescence spectra. Because of this arrangement, there is an intensity limitation on the experiment because only a small portion of the emission is collected.

There is also an intrinsic problem that arises for site selection if the sites are closer than either the laser bandwidth or the spectral linewidth. This spectral

